Ligand-Induced Conformational Change in the Ferric Enterobactin Receptor FepA As Studied by Site-Directed Spin Labeling and Time-Domain ESR†

Candice S. Klug,‡ Sandra S. Eaton,§ Gareth R. Eaton,§ and Jimmy B. Feix*,‡

Biophysics Research Institute, Medical College of Wisconsin, 8701 Watertown Plank Road, Milwaukee, Wisconsin 53226, and Department of Chemistry and Biochemistry, University of Denver, Denver, Colorado 80208

Received January 20, 1998; Revised Manuscript Received April 27, 1998

ABSTRACT: A mutant of the ferric enterobactin receptor, FepA, containing a valine to cysteine (V338C) substitution was made and the purified protein selectively modified with a sulfhydryl-specific nitroxide spin label. In reconstituted liposomes, interaction of the attached spin label with a combination of water-soluble and lipid-soluble relaxation agents indicated that the V338C site was located in the polar headgroup region of the membrane, approximately 1.5−4.5 Å above the phosphate groups of the lipids. Binding of the ligand, ferric enterobactin (FeEnt), to the purified spin-labeled protein produced a significant decrease in both the rotational freedom and accessibility of the nitroxide, indicating the formation of new structural contacts between the spin label and either the protein or the bound ligand. Electron spin−echo (ESE) measurements of the nitroxide phase-memory relaxation rate in the presence and absence of bound ligand showed substantial dipolar coupling between the Fe^{3+} of FeEnt and the spin label and provided an iron−nitroxide distance estimate in the range of 20−30 Å. We conclude that the ligand-induced changes in spin label motion and accessibility are due to new tertiary contacts with the protein and not to direct contact with the ligand. These studies suggest that V338C may occupy a hinge region connecting the ligand binding surface loop to the β-barrel and provide the strongest evidence to date of an in vitro ligand-induced conformational change in FepA.

The mechanisms of gating and transport are key aspects of the function of any ligand-gated receptor. The ferric enterobactin receptor FepA is an 81 kDa ligand-gated channel that mediates iron transport across the outer membrane (OM) of *Escherichia coli* and many related Gram-negative bacteria via the binding and translocation of Fe^{3+} bound to the catecholate ligand enterobactin (*1*). Although ferric enterobactin (FeEnt)[1] binds to FepA in vitro, its transport across the OM requires an intact electrochemical potential across the bacterial inner membrane (*2*) and participation of the inner membrane protein, TonB (*3*−*5*), in addition to several cytoplasmic membrane proteins (reviewed in *6*). The mechanisms that couple FeEnt transport with the inner membrane potential and govern FepA−TonB interaction are not known.

Based on analogy to crystallized porins (e.g., *7*−*9*) and hydrophobicity analysis (*10*), FepA is thought to contain a transmembrane β-barrel composed of antiparallel β-strands that surround a central aqueous channel. It has been suggested that all Gram-negative bacterial OM channel proteins are based on this general motif (*11*). FeEnt binds to a large extracellular surface loop of FepA that not only contains the FeEnt binding site but also keeps the transmembrane channel in a closed configuration (*12*, *13*). We have confirmed β-strand secondary structure for one of the putative transmembrane strands (*14*), verifying the β-barrel hypothesis. In that study, we used the site-directed spin labeling (SDSL) technique to show that the accessibility of residues in the strand to both water- and lipid-soluble relaxation agents varied with a periodicity of 2; alternating sites are exposed to the channel lumen and the hydrophobic phase of the lipid bilayer.

SDSL (reviewed in *15*) is emerging as a powerful technique for the study of protein structure and dynamics. This approach involves utilizing site-directed mutagenesis to substitute a cysteine residue at a desired labeling site followed by reaction of the cysteine with a sulfhydryl-specific nitroxide spin label. The ability to introduce cysteine residues at desired locations, rather than relying on endogenous labeling sites, greatly enhances the applicability of the spin labeling method and allows the independent study of multiple sites in a given protein. The spectroscopic information obtained on the physical environment of the mutated site provides structural insights that cannot be obtained by site-directed mutagenesis and functional analysis alone. SDSL is particularly applicable to large membrane proteins that are not amenable to NMR analysis and which do not readily crystallize (reviewed in *16*). SDSL can provide

† Supported by NIH Grants GM22923, GM51339 (J.B.F.), GM21156 (G.R.E. and S.S.E.), and RR01008.

* To whom correspondence should be addressed at the Biophysics Research Institute, Medical College of Wisconsin, 8701 Watertown Plank Rd., Milwaukee, WI 53226. FAX: 414-456-6512.

‡ Medical College of Wisconsin.

§ University of Denver.

[1] Abbreviations: CW, continuous wave; CROX, chromium(III) oxalate; ESE, electron spin−echo; ESR, electron spin resonance; FeEnt, ferric enterobactin; MTSL, methanethiosulfonate spin label; MOPS, 3-(*N*-morpholino)propanesulfonic acid; NiAA, nickel(II) acetylacetonate; NiEDDA, nickel(II) ethylenediaminediacetate; PAGE, polyacrylamide gel electrophoresis; SDS, sodium dodecyl sulfate; TCEP, tris(2-carboxyethyl)phosphine; ZFS, zero-field splitting.

S0006-2960(98)00144-5 CCC: $15.00
Published on Web 06/05/1998

information on the location of a given site relative to the membrane bilayer, the tertiary structure surrounding the attached label, and local conformational changes induced by chemical or physiological perturbations.

Previously, we used the SDSL technique to demonstrate that even in the absence of TonB, binding of FeEnt to FepA causes a conformational change in the large, extracellular surface loop that has been shown to contain the ligand binding site (*17*). In the present work, we show that FeEnt binding induces a significant conformational change at a site that is putatively part of the β-barrel domain and not part of the ligand binding surface loop. FeEnt binding results in a structural alteration that greatly restricts the rotational mobility of an attached nitroxide spin label at this site and diminishes accessibility to water-soluble relaxation agents in the aqueous phase. Measurement of the distance from the bound ferric iron to the spin label by electron spin−echo (ESE) spectroscopy indicates a separation of 20−30 Å, demonstrating that the ligand-induced restrictions on spin label motion and accessibility are due to altered tertiary contacts between the nitroxide and the protein and not to direct contact between the spin label and the bound ligand. These studies provide the strongest evidence to date of an in vitro ligand-induced conformational change in FepA.

MATERIALS AND METHODS

Mutagenesis and Protein Purification. The single cysteine V338C mutation was created and verified as previously described (*14*). Protein was purified from *E. coli* RWB18-60 (*18*) harboring a pUC19-based plasmid encoding the FepA gene (*19*) as previously published (*20*−*22*).

Site-Directed Spin Labeling. The purified protein was labeled at the introduced cysteine residue with the sulfhydryl-specific spin label (1-oxy-2,2,5,5-tetramethylpyrroline-3-yl)-methyl methanethiosulfonate (MTSL, Reanal, Budapest, Hungary) at a 2−10-fold molar excess overnight at 4 °C. Excess spin label was removed by dialysis. The two native cysteines in FepA are involved in a disulfide bond and do not spin-label without the prior addition of a thiol reducing agent (*17*), thus leaving the singly introduced cysteine the only labeled site. Spin quantitation was carried out by incubating an aliquot of MTSL-labeled V338C in 10 mM tris(2-carboxyethyl)phosphine (TCEP, Molecular Probes, Eugene, OR), which cleaves the spin label−protein disulfide bond and releases the nitroxide into the solution. The spin concentration was determined by double integration of the resulting spectrum and comparison with a standard nitroxide solution. Protein concentration was determined from the absorbance at 280 nm using an extinction coefficient of 1.56 $\times 10^5$ M^{-1} cm^{-1} based on amino acid composition (*23*). The labeling efficiency of V338C with MTSL was determined to be 0.76.

ESR Sample Preparation. For CW ESR studies on the effects of ligand binding, purified MTSL-V338C suspended in 20 mM MOPS/2% Triton X-100, pH 7, at a concentration of approximately 0.2 mM was mixed with FeEnt and any appropriate relaxation agent (e.g., NiAA) in the same buffer to give a 2-fold excess of FeEnt in a final volume of 10 μL. Samples were placed in a gas-permeable TPX capillary (*24*), and the ESR spectra and power saturation curves were obtained at room temperature. For time-domain ESR studies, 100 μL of solution containing 0.2 mM MTSL-V338C or wild-type FepA was mixed with a 2−5-fold molar excess of FeEnt, and the ligand was allowed to bind at room temperature. This concentration of FeEnt is high enough to ensure that each FepA monomer contains a bound ligand, but is sufficiently low that unbound ligand should have no significant effects on spin label relaxation times. After allowing the ligand to bind, samples were mixed with an equal volume of glycerol as cryoprotectant, placed in 4 mm OD quartz tubes, and deoxygenated by three freeze−pump−thaw cycles, and the tubes were back-filled with helium gas. Samples were stored in liquid nitrogen and kept frozen during insertion into the spectrometer cryostat.

Liposome Preparation. Multilamellar liposomes containing egg phosphatidylcholine and 1-palmitoyl-2-oleoylphosphatidylglycerol at a molar ratio of 5:1 and MTSL-V338C (lipid:protein ratio approximately 800:1) were prepared as described previously (*14*). Aqueous relaxation agents (i.e., CROX, NiAA, NiEDDA) were included in the final suspension buffer so that all lamellae were exposed to an equal concentration of these reagents. NiAA and CROX were from Aldrich Chemical Co. (Milwaukee, WI), and the NiEDDA synthesis protocol used was kindly provided by Dr. C. Altenbach (University of California, Los Angeles).

Continuous Wave (CW) ESR Measurements. CW ESR measurements were made on a Varian E102 Century Series spectrometer (Varian Associates, Palo Alto, CA) equipped with a loop-gap resonator (Medical Advances, Milwaukee, WI) using 1 mW microwave power and 1.0 G field modulation. Signal averaging and data analysis were done using the programs Viking and SUMSPC92 (National Biomedical ESR Center, Milwaukee), respectively. CW power saturation studies were done with 1.25 G field modulation, and the incident power (P) typically varied from 0.1 to 36 mW. Power saturation curves were fit to the function:

$$A = IP^{1/2}[1 + (2^{1/\epsilon} - 1)P/P_{1/2}]^{-\epsilon} \qquad (1)$$

(*25*) where A is the amplitude of the first-derivative center line, I is a scaling factor, ϵ is a homogeneity factor, and $P_{1/2}$, the half-saturation parameter, is the power at which the signal intensity is half that which it would be in the absence of saturation. Φ and depth calculations were carried out as previously described (*14*).

Time-Domain ESR Measurements. Electron spin−echo (ESE) and inversion recovery measurements were made on a Bruker ESP380E spectrometer equipped with an ER4118X-MS5 split-ring resonator and an Oxford CF935 liquid helium cryostat as described previously (*26*, *27*). The Oxford cryostat readout was calibrated by placing a TG-120PL GaAlAs diode immersed in silicone oil in a 4 mm quartz tube in the sample cavity. The uncertainty in temperature is estimated at ±1 K. The split-ring resonator was over-coupled to a Q of approximately 150, bringing the spectrometer deadtime to 64 ns. Inversion recovery data were obtained using a $\pi-T-\pi/2-\tau-\pi-\tau-$echo sequence in which the time, T, was varied. Pulse lengths were 16 and 24 ns, and the microwave field intensity and τ values were selected to provide maximum echo intensity. Inversion recovery curves were fitted to a sum of exponentials using the algorithm developed by Provencher (*28*).

ESE data were obtained using a $\pi/2-\tau-\pi-\tau-$echo sequence with 40 and 80 ns pulses. For the nitroxide signal and for the iron signal at magnetic fields greater than 2900 G, ESE decay curves were fitted to the equation:

$$Y(\tau) = Y(0)\exp[-(2\tau/T_m)^x] \quad (2)$$

(*29*) using a Levenberg−Marquardt least-squares algorithm where $Y(\tau)$ is the echo intensity, $Y(0)$ is the echo intensity extrapolated to time zero, T_m is the phase-memory relaxation time, and x is a parameter that describes the shape of the decay curve. T_m encompasses all processes that lead to echo dephasing, including metal-induced dipolar relaxation. At magnetic fields below about 2900 G, the echo decays for the iron signal exhibited substantial echo envelope modulation so the value of T_m was determined by fitting the decays to a product of a decay function and an echo modulation function.

Iron−Nitroxide Distance Measurement. The analysis of nitroxide spin−echo decays to determine the distance between low-spin Fe^{3+} ($S = {}^1/_2$) and a nitroxide has been reported (*26, 27*). In those cases the iron relaxation is a two-site exchange. For high-spin Fe^{3+} ($S = {}^5/_2$), as in the FeEnt complex, the iron relaxation is a six-site exchange between values of m_s ranging from −5/2 to +5/2. Since equations are not yet available to analyze the nitroxide spin−echo decays for this case, two approximate approaches were used to estimate the interspin distance. First, when the iron−nitroxide distance is shorter than about 15 Å, the collapse of the iron−nitroxide splitting due to increasing rates of iron relaxation makes the nitroxide T_m so short that most of the echo intensity decays within the spectrometer deadtime (*30*). Our ability to observe echo decays indicates that T_m is not this short for the nitroxide in FeEnt+MTSL-FepA, and we conclude that the nitroxide is not in the immediate vicinity of the iron. As the iron-nitroxide distance increases, the maximum value of the nitroxide T_m^{-1} decreases and the intensity of the echo at the temperature corresponding to the maximum value of T_m^{-1} increases. After correcting for the Boltzmann dependence of echo intensity, the nitroxide echo intensity for FeEnt+MTSL-FepA at $\tau = 200$ ns and $T = 60$ K was about one-fourth of that observed at 6 K. For spin-labeled high-spin metmyoglobins with iron−nitroxide distances of about 17 Å, the nitroxide echo intensity at $\tau =$ 200 ns, the temperature at which T_m^{-1} was largest, was about one-sixth of that at low temperature (Zhou, Eaton, and Eaton, unpublished results). Thus, the iron−nitroxide distance in FeEnt+MTSL-FepA must be significantly longer than 17 Å, and we estimate that it must be longer than at least 20 Å. The observation of the substantial effect of the iron on the nitroxide T_m^{-1} and on echo intensity requires that the iron−nitroxide distance is less than about 30 Å. Second, the multisite exchange was approximated as two-site exchange with a dipolar splitting proportional to $\sqrt{S(S+1)}$. Simulation of the echo decays using the equations in ref. *26* and *27* and values of the iron relaxation rates extrapolated from the data in Figure 4 were consistent with an interspin distance of about 25 Å.

RESULTS

Functional Analysis of V338C. FepA mutant V338C was expressed, and the cells showed FeEnt-dependent growth at wild-type levels. In addition, the susceptibility of cells expressing V338C to colicin B, a toxin for which FepA is also a receptor, was similar to wild type. Thus, these results indicate that the ligand binding site and transmembrane channel were not significantly altered by the mutation and also show that FepA containing the V338C mutation is able to interact effectively with TonB. Both FepA-V338C and wild-type FepA ran with an anomalously low apparent molecular mass of 68 kDa on SDS−PAGE due to the compact nature of the β-barrel structure, indicating that the mutant was properly folded. The effects of FeEnt binding on the CW spectrum of MTSL-V338C (discussed below) clearly show that the purified, spin-labeled protein retains ligand binding activity. The minimal impact of the mutation on protein structure is consistent with the work of Hubbell, Khorana, and co-workers, who have established that for bacteriorhodopsin and rhodopsin, single cysteine mutations at numerous sites cause minimal disruption of the native structure (e.g., *31*−*33*). Similarly, Matthews and co-workers have established the resilience of the T4 lysozyme to multiple single-site mutations (reviewed in *34*).

CW ESR Studies. To establish the location of V338C relative to the lipid bilayer, we used CW power saturation to measure the accessibility of the attached spin label of purified MTSL-V338C to the water-soluble relaxation agents NiAA, NiEDDA, and CROX and to the nonpolar, lipid-soluble relaxation agent O_2 in reconstituted liposomes (Table 1). Although NiAA and NiEDDA partition primarily into the aqueous phase, they have depth-dependent concentrations in the lipid bilayer. High accessibility to all of the water-soluble relaxation agents was observed, indicating exposure to the aqueous phase. Calculation of the depth parameter Φ indicated a location 1.2−4.5 Å above the phosphate groups of the lipids. Based on these results and sequence analysis, V338C likely occupies a site within the polar headgroup region of the bilayer at the top (extracellular surface) of a transmembrane β-strand.

Binding of FeEnt to MTSL-V338C produced a substantial change in the structure surrounding the labeled site, as indicated by both conventional and power saturation ESR. The ESR spectrum of MTSL-V338C in Triton X-100 detergent micelles is shown in Figure 1A. The spectrum indicates the presence of two spin label populations that are of approximately equal intensity; one is immobilized on the ESR time scale (closed arrow), and one has rotational mobility in the intermediate range with rotational correlation times on the order of 10 ns (open arrow), reflecting the ability of the spin label to adopt alternate conformations relative to the peptide backbone (*35*). FeEnt binding to MTSL-V338C alters the structure of the site such that the entire population of spin labels is very strongly immobilized, as indicated by the formation of a distinct powder pattern with resolution of the minor **g** and **A** tensor splittings in the central line (Figure 1B).

Changes in the local environment of MTSL-V338C upon ligand binding were also apparent in CW saturation studies (Table 2). Without bound ligand, the ESR signal for MTSL-V338C saturated in the presence of NiAA gives a $\Delta P_{1/2}$ of 24.9 mW (Table 2), indicating the extremely high accessibility of this site to the aqueous phase and consistent with its localization near the extracellular surface of the β-barrel. After binding FeEnt, the accessibility of MTSL-V338C to

Table 1: Accessibility Parameters and Depth Calculations in Liposomes[a]

	$\Delta P_{1/2}$							
mutant	(O_2)[b]	CROX	NiAA	NiEDDA	Φ(NiAA)	depth(NiAA) (Å)	Φ (NiEDDA)	depth(NiEDDA) (Å)
V338C	2.01	6.67	6.05	19.67	−1.11	−1.2	−2.28	−4.5

[a] Power saturation parameters reflecting accessibility and bilayer depth for MTSL-V338C in reconstituted liposomes. [b] $\Delta P_{1/2}$ parameters were obtained in the presence of air (20% oxygen), 20 mM CROX, 20 mM NiAA, or 200 mM NiEDDA, as described in the text. See (*14*) for Φ and depth calculations.

Table 2: Accessibility Data for MTSL-V338C in Detergent Micelles in the Presence and Absence of Ligand[a]

	−FeEnt			+FeEnt		
mutant	$P_{1/2}(N_2)$	$\Delta P_{1/2}(O_2)$	$\Delta P_{1/2}$(NiAA)	$P_{1/2}(N_2)$	$\Delta P_{1/2}(O_2)$	$\Delta P_{1/2}$(NiAA)
V338C	3.47	3.05	24.9	2.43	1.50	15.1

[a] Power saturation parameters reflect the change in accessibility of MTSL-V338C upon FeEnt binding in Triton X-100 micelles. The decrease in $P_{1/2}(N_2)$ in the presence of FeEnt is due to the increase in nitroxide spin−lattice relaxation time (T_1) that accompanies the decrease in motion (i.e., increased rotational correlation time, τ_c) seen in Figure 1 (*49*). The decreased values of $\Delta P_{1/2}(O_2)$ and $\Delta P_{1/2}$(NiAA) in the presence of FeEnt reflect the lower accessibility of the spin-labeled site to these relaxation reagents.

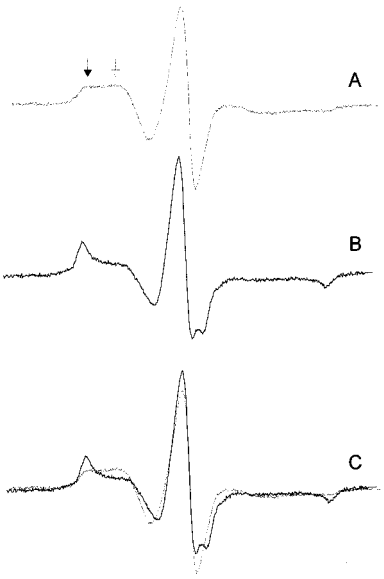

FIGURE 1: Ligand-induced change in spin label motion for MTSL-V338C. CW ESR spectra of purified MTSL-V338C in MOPS/Triton X-100 (A) in the absence of ligand, (B) saturated with FeEnt, and (C) overlay. Spectra were recorded at room temperature with a field sweep of 100 G.

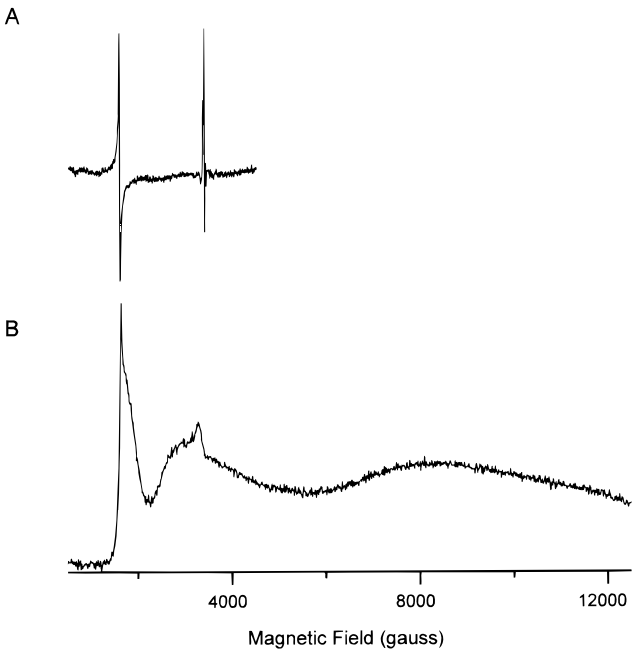

FIGURE 2: (A) First-derivative CW ESR spectrum of MTSL-V338C bound to FeEnt obtained at 15 K with a microwave power of 0.010 mW and a modulation amplitude of 3.1 G. (B) Echo-detected ESR absorption spectrum of the same sample at 6 K.

NiAA was markedly diminished (Table 2), and accessibility to O_2 was also decreased (Table 2). FeEnt binding had little effect on the unperturbed $P_{1/2}(N_2)$. This is entirely expected given that the Fe^{3+} relaxation times at room temperature are on the order of a nanosecond or less, which is too fast for effective dipolar coupling to the nitroxide. Thus, the changes in $\Delta P_{1/2}$ for O_2 and NiAA upon ligand binding reflect changes in the accessibility of the nitroxide and not relaxation enhancement by the bound ligand complex. Interaction of MTSL-V338C with NiAA in the ligand-bound state was still significantly greater than observed for sites located in the nonpolar phase of the micelle (*14*), and the relative interaction rates with O_2 and NiAA indicate that the spin-labeled site remained in the polar headgroup region of the bilayer upon ligand binding. The reduced accessibilities of MTSL-V338C to O_2 and NiAA show that new structural interactions induced by ligand binding produce a change in the environment of the spin label and are consistent with the observed decrease in rotational mobility (Figure 3). These new structural interactions may be either additional tertiary contacts of the spin label with the protein or direct contact between the nitroxide and FeEnt itself. In addition, several sites in an adjacent β-strand also show changes in the motion and accessibility upon FeEnt binding (Klug and Feix, unpublished data).

Time-Domain ESR Studies. To examine the interaction between the Fe^{3+} center of the bound ligand and the nitroxide attached to FepA, time-domain ESR measurements were performed. The first-derivative ESR signal at 15 K for MTSL-V338C bound to FeEnt is shown in Figure 2A. The prominent feature at ∼1700 G is typical of high-spin Fe^{3+} in a low-symmetry environment and has been described previously for FeEnt (*36*). The signal at 3500 G is due to the nitroxide and is substantially power-saturated under the conditions employed, which are optimized to detect Fe^{3+}. Figure 2B shows the two-pulse echo-detected ESR absorption signal for the same system at 6 K. Although the first-

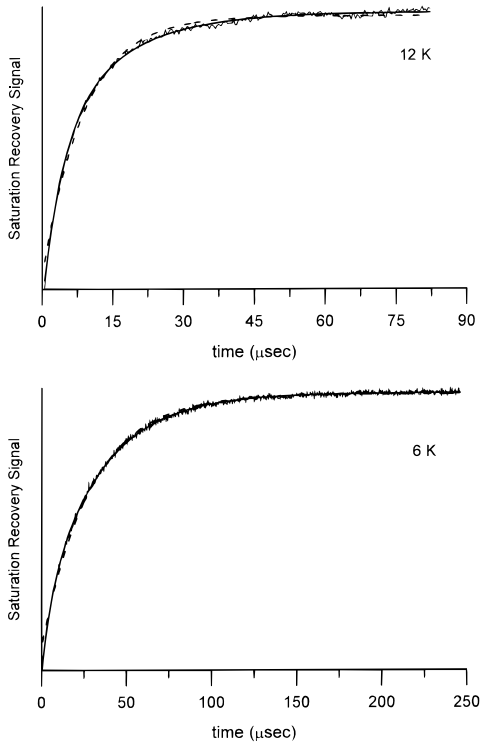

FIGURE 3: Inversion recovery curves for the high-spin Fe^{3+} in FeEnt bound to FepA at 6 K (2000 G) and 12 K (1730 G). The solid lines are fits to a single exponential, and the dashed lines are fits to the sum of two exponentials. Resulting T_1 values are plotted in Figure 4.

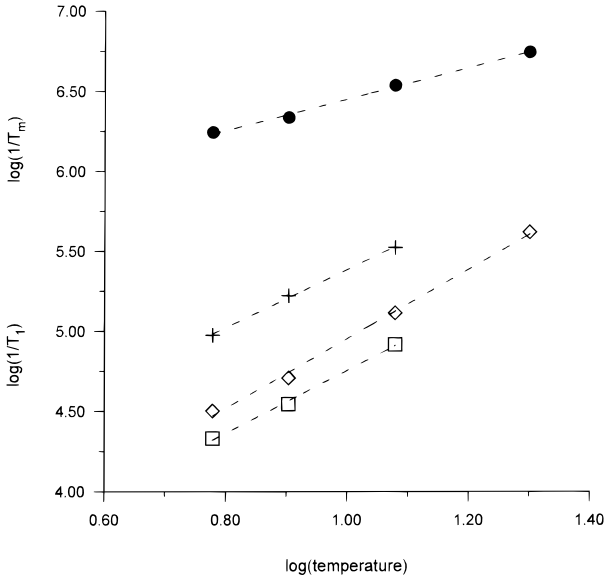

FIGURE 4: Temperature dependence of electron spin relaxation rates for Fe^{3+} in FeEnt bound to wt-FepA: T_m^{-1} from two-pulse spin−echo data (●), T_1^{-1} obtained by fitting inversion recovery data to a single exponential (◇), and slow (□) and fast components (+) of T_1^{-1} obtained by fitting inversion recovery data to a sum of two exponentials. The average values of T_m^{-1} and T_1^{-1} obtained at several points in the spectrum were used to generate the plots. Dashed lines are least-squares fits to the data: $\text{Log}(T_m^{-1}) = 1.07 \log(T) + 5.36$; single-exponential fit, $\log(T_1^{-1}) = 2.17 \log(T) + 2.78$; short component, $\log(T_1^{-1}) = 1.81 \log(T) + 3.57$; long component, $\log(T_1^{-1}) = 1.96 \log(T) + 2.79$.

derivative spectrum (Figure 2A) exhibited features attributable to the Fe^{3+} only in the vicinity of 1700 G, the signal intensity for the Fe^{3+} in the absorption spectrum extends from 1500 to >12 500 G (the maximum spectrometer field) because the absorption spectrum facilitates observation of signals for which intensity varies slowly with magnetic field. The observation of signal intensity extending beyond 12 500 G indicates that the zero-field splitting (ZFS) for Fe^{3+} is greater than the X-band EPR quantum (∼0.3 cm^{-1}) and is consistent with the literature report of ZFS = 0.50 cm^{-1} for FeEnt (*37*).

Values of the spin−lattice relaxation time (T_{1e}) of Fe^{3+} in FeEnt bound to wt FepA, which are required for distance calculations, were determined by inversion recovery ESR at 3−6 magnetic field strengths and varied by less than 30% with position in the spectrum. Fits to a single exponential were not as good as fits to the sum of two exponentials. The sum of two exponentials cannot be distinguished readily from a distribution in exponential time constants, which can arise from a distribution in zero-field splittings. Typical inversion recovery curves for the Fe^{3+} center are shown in Figure 3, and the temperature dependence of T_{1e}^{-1} is shown in Figure 4. The temperature dependence of values of T_m^{-1} for the Fe^{3+} center obtained by two-pulse spin−echo is also included in Figure 4. For Fe^{3+} in a magnetically dilute sample such as these protein samples, T_m is approximately equal to T_2.

Typical nitroxide ESE decay curves for MTSL-V338C in the presence and absence of FeEnt are shown in Figure 5A and 5B, respectively. In the absence of FeEnt, the echo decay was approximately independent of temperature between 10 and 70 K (Figure 6), which is typical for nitroxide

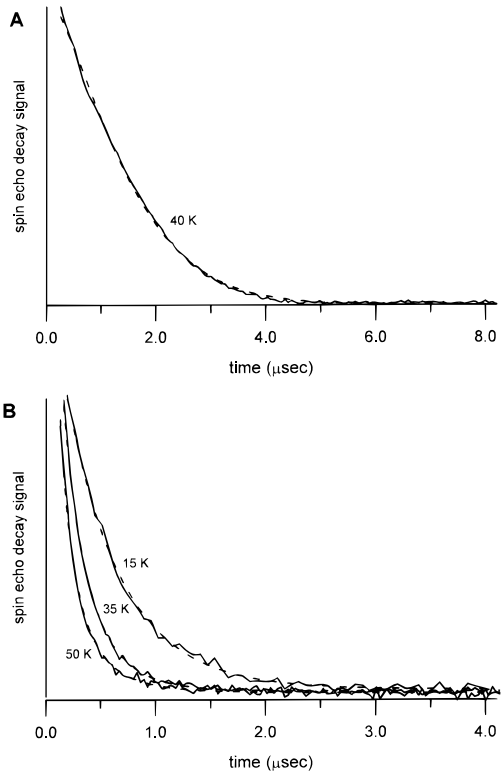

FIGURE 5: Two-pulse electron spin−echo decays obtained in the center of the nitroxide spectrum for (A) MTSL-V338C at 40 K and (B) MTSL-V338C containing bound FeEnt at 15, 35, and 50 K. The dashed lines are fits of the data to eq 2 (see text). Note that the time axis for part A is twice as long as that for part B.

radicals in this temperature regime (*26*, *29*, *38*). The echo decay curves were fitted to eq 2 (see Materials and Methods)

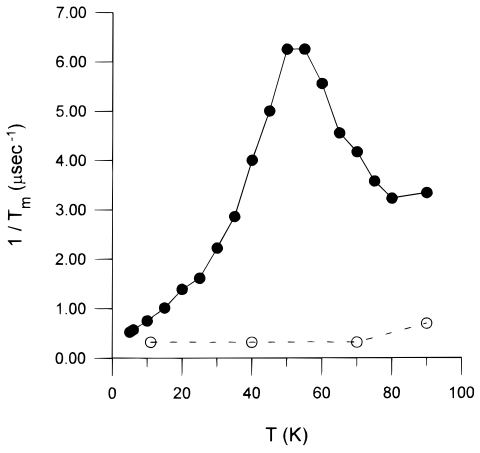

FIGURE 6: Spin label phase-memory relaxation rates (T_m^{-1}) as a function of temperature for MTSL-V338C in the presence (●) and absence (○) of bound FeEnt obtained from two-pulse ESE measurements. T_m values were obtained by fitting echo decays to eq 2 as described under Materials and Methods.

with $T_m = 3.1$ μs and $x = 1.4$. These parameters are characteristic of a nitroxide in an environment containing a substantial concentration of methyl groups (*29*), indicating that the spin label is in the immediate vicinity of protein and is not fully surrounded by the H_2O/glycerol solvent, again consistent with the restricted mobility of the spin label observed in Figure 3. The small increase in T_m^{-1} observed at 90 K is due to the increasing rate of rotation of the methyl groups on the nitroxide ring. The rotation of these groups at rates comparable to the electron−methyl−proton couplings dominates the echo dephasing between about 100 and 150 K (*38*).

In the presence of bound FeEnt, the echo decay curves for the nitroxide in MTSL-V338C displayed a strong temperature dependence between 4 and 70 K (Figure 5). To obtain a qualitative description of the temperature dependence, data were fitted to eq 2. The values of T_m^{-1} increased up to about 50−55 K and then decreased (Figure 6). The value of x (in eq 2) decreased from 1.1 at low temperature to 0.55 at 50−55 K and then increased to 0.8 at 90 K. This temperature dependence of both T_m^{-1} and x is characteristic of the changes that occur when the rate of a dynamic process involving a spin that is coupled to the unpaired electron of the nitroxide goes from slow to intermediate compared with the magnitude of the coupling. Similar changes in T_m^{-1} and x have been observed for nitroxides that are coupled to low-spin (*26*, *27*) and high-spin (*30*, *39*) Fe^{3+} hemes and porphyrins. The dynamic process in these systems is the iron electron spin relaxation, and the coupling that is averaged by the dynamic process is the electron−electron spin−spin coupling. The increase in nitroxide T_m^{-1} occurs as $\tau_c = \sqrt{T_{1f}T_{2f}}$ decreases from about 10^{-6} to 10^{-7} s, where τ_c is the correlation time for the dynamic process, and T_{1f} and T_{2f} are T_1 and T_2 for the Fe^{3+}. Extrapolation of the experimental relaxation times for the Fe^{3+} in wt-FepA+FeEnt (Figure 4) to higher temperatures indicates that $\sqrt{T_{1f}T_{2f}}$ decreases from about 10^{-6} to 10^{-7} s between about 15 and 60 K, which is also the temperature interval where the increase in nitroxide T_m^{-1} was observed (Figure 6). Thus, the iron relaxation rates for FeEnt bound to FepA are consistent with assignment of the changes in the nitroxide T_m^{-1} in the complex of FeEnt with MTSL-FepA to interaction with the iron.

The iron−nitroxide distance can be determined by analysis of the temperature-dependent nitroxide spin−echo decay shapes in the regime where the metal relaxation rate is comparable to the magnitude of the spin−spin splitting (*26*, *27*). For the Fe^{3+} in FeEnt+MTSL-FepA, the analysis is complicated by the fact that high-spin Fe^{3+} has $S = 5/2$ and in the limit of slow iron relaxation each nitroxide transition is split into a multiplet. Analysis of the collapse of these splittings is more complicated than the two-site exchange required for interaction with an $S = 1/2$ metal (*26*, *27*). As described under Materials and Methods, approximate analyses of the nitroxide spin−echo data indicate that the iron−nitroxide distance is 20−30 Å. Further work is in progress to obtain a more precise value of the iron−nitroxide distance in this system.

The crystal structure of vanadium(IV) enterobactin (VEnt) indicates that the distance between the metal atom and the surface of the VEnt complex varies between 3 and 7.5 Å (*40*). The structure of the FeEnt complex is expected to be similar to that for VEnt; thus, the 20−30 Å iron−nitroxyl distance estimated for FeEnt bound to FepA is much longer than would be observed if the FeEnt were in direct contact with the spin-labeled site. This comparison supports the proposal that the decreased mobility of the spin label that is observed when FeEnt binds to FepA is due to changes in the tertiary structure of the protein rather than direct contact between FeEnt and the spin-labeled site.

DISCUSSION

The mechanism of FeEnt transport across the bacterial OM is currently unknown. However, it appears to be a multistep process involving ligand binding, opening of the channel, and release of the ligand into the aqueous channel lumen. Since FeEnt binds to the resting FepA channel with high affinity ($K_d \approx 20$ nM; *1*, *41*), a conformational change in the receptor would appear to be a necessary step in facilitating ligand release. Such a step could occur in response to ligand binding or as a result of FepA−TonB interaction. Cross-linking studies with glutardialdehyde have indicated that at least some population of the two proteins are in close physical proximity (*42*, *43*). Interaction between TonB and FepA could occur randomly as a consequence of the lateral diffusion of TonB in the inner membrane (lateral diffusion in the OM being highly limited due to its rigid structure), or selectively between TonB and FepA occupied with bound ligand. Thus, it is important to establish whether structural changes occur in FepA in the absence of TonB. In this work, we have shown that ligand binding alone to the purified receptor is sufficient to induce a substantial conformational change in FepA and could serve as a transmembrane signaling mechanism for TonB interaction.

An interesting aspect of this study is that V338 is not part of the primary sequence which constitutes the ligand binding site. Mapping of MTSL-V338C in reconstituted liposomes by power saturation methods indicates that it is in the polar headgroup region of the bilayer, and hydrophobicity analysis of the FepA sequence (*10*) locates V338 at the top of a β-strand. Consequently, the location of this site places it in a potential hinge region between the ligand binding domain

and the β-barrel, in excellent position to interact with the surface loop(s) involved directly in ligand binding.

Time-domain and CW ESR methods to measure metal−nitroxide distances enhance the detailed structural information that can be obtained by SDSL. Either approach is applicable to metalloproteins containing a native paramagnetic metal ion or to proteins containing engineered metal binding sites (e.g., *44*−*46*), provided that the appropriate conditions are satisfied. The Leigh method relies on a decrease in amplitude of the spin label spectrum as a result of broadening due to dipolar coupling to a nearby (<25 Å) metal (*44*) and has been applied to mapping distances in many species (*47*) including T4 lysozyme (*45*) and the *E. coli* lactose permease (*46*). Application of that technique requires exactly comparable CW EPR spectra in the presence and absence of the metal ion. In the FepA case, binding of the FeEnt causes conformational changes in FepA, making it difficult to obtain an appropriate comparison spectrum in the absence of iron. In addition, application of the Leigh model requires that data are analyzed in a temperature regime where the metal relaxation rate, T_1^{-1}, is comparable to the metal−nitroxide dipolar interaction in s^{-1} (*47*, *48*). For the iron−nitroxide distances and iron relaxation rates that we estimate for FeEnt bound to MTSL-V338C, this requirement would necessitate obtaining nitroxide CW spectra at temperatures between about 40 and 60 K. At these low temperatures, the nitroxide relaxation rates become very slow, making it difficult to obtain unsaturated CW spectra. Since the iron−nitroxide interaction changes the nitroxide relaxation rate, one cannot simply obtain spectra in the presence and absence of iron at the same microwave power and assume comparable degrees of saturation. In addition, at the long interspin distances for this system, the predicted Leigh effect on signal amplitude is small, increasing uncertainties in the measurements. For these reasons, we did not attempt to apply the Leigh method to this system.

Time-domain methods that directly measure the effects of the metal on the spin label relaxation times (e.g., *26*, *27*, and references cited therein) do not require the rigorous attention to spin quantitation required by CW methods. Another fundamental difference between CW and time-domain measurements is that the spin−echo studies examine changes in spin-packet widths whereas CW studies examine changes in inhomogeneously broadened line shapes. In systems rich in nuclear spins (including protons), spin-packet widths are typically much narrower than the inhomogeneously broadened line widths, making time-domain studies more sensitive than CW measurements to the small effects of dipolar interactions at long distances. In the present study, the estimation of a metal−nitroxide distance provided information on the separation between a given spin-labeled site and the bound paramagnetic ligand and allowed us to distinguish between effects due to direct interaction of the ligand with the spin-labeled site and a conformational change in the protein due to binding of the ligand that impacted the spin-labeled site.

In conclusion, the binding of FeEnt to purified FepA produces a conformational change in the receptor that alters the extent of tertiary interactions at V338C, a site at the membrane surface in a β-strand that is not directly a part of the surface loop containing the ligand binding site. Time-domain ESR data confirm that the changes in motion and accessibility of a nitroxide spin label attached at this site are due to a structural rearrangement in FepA and not due to contact between the spin label and bound ligand. These studies demonstrate that ligand binding alone is sufficient to induce alterations in purified FepA that impact the receptor structure at sites beyond those comprising the surface loop containing the ligand binding site. Further studies on the extent to which this change is transmitted throughout the FepA structure will help determine its role in receptor gating, FepA−TonB interaction, and the translocation of FeEnt through the transmembrane channel.

REFERENCES

1. Hollifield, W. C., Jr., and Neilands, J. B. (1978) *Biochemistry 17*, 1922−1928.
2. Pugsley, A. P., and Reeves, P. (1976) *J. Bacteriol. 114*, 1225−1230.
3. Wang, C. C., and Newton, A. (1971) *J. Biol. Chem. 246*, 2147−2151.
4. Postle, K. (1990) *Mol. Microbiol. 4*, 2019−2025.
5. Braun, V. (1995) *FEMS Microbiol. Rev. 16*, 295−307.
6. Guerinot, M. L. (1994) *Annu. Rev. Microbiol. 48*, 743−772.
7. Weiss, M. S., Abele, U., Weckesser, J., Welte, W., Schiltz, E., and Schulz, G. E. (1991) *Science 254*, 1627−1630.
8. Cowan, S. W., Schirmer, T., Rummel, G., Steiert, M., Ghosh, R., Pauptit, R. A., Jansonius, J. N., and Rosenbusch, J. P. (1992) *Nature 358*, 727−733.
9. Schirmer, T., Keller, T. A., Wang, Y.-F., and Rosenbusch, J. P. (1995) *Science 267*, 512−514.
10. Murphy, C. K., Kalve, V. I., and Klebba, P. E. (1990) *J. Bacteriol. 172*, 2736−2746.
11. Nikaido, H., and Saier, M. H., Jr. (1992) *Science 258*, 936−942.
12. Rutz, J. M., Liu, J., Lyons, J. A., Goranson, J., Armstrong, S. A., McIntosh, M. A., Feix, J. B., and Klebba, P. E. (1992) *Science 258*, 471−475.
13. Liu, J., Rutz, J. M., Feix, J. B., and Klebba, P. E. (1993) *Proc. Natl. Acad. Sci. U.S.A. 90*, 10653−10657.
14. Klug, C. S., Su, W., and Feix, J. B. (1997) *Biochemistry 36*, 13027−13033.
15. Hubbell, W. L., and Altenbach, C. (1994) *Curr. Opin. Struct. Biol. 4*, 566−573.
16. Feix, J. B., and Klug, C. S. (1998) in *Spin Labeling: The Next Millenium* (Berliner, L. J., Ed.) pp 251−281, Plenum, New York.
17. Liu, J., Rutz, J. M., Klebba, P. E., and Feix, J. B. (1994) *Biochemistry 33*, 13274−13283.
18. Leong, J., and Neilands, J. B. (1976) *J. Bacteriol. 126*, 823−830.
19. Armstrong, S. K., Francis, C. L., and McIntosh, M. A. (1990) *J. Biol. Chem. 265*, 14536−14543.
20. Neidhardt, F. C., Bloch, P. L., and Smith, D. F. (1974) *J. Bacteriol. 119*, 736−747.
21. Fiss, E. H., Stanley-Samuelson, P., and Neilands, J. B. (1982) *Biochemistry 21*, 4517−4522.
22. Klug, C. S., Su, W., Liu, J., Klebba, P. E., and Feix, J. B. (1995) *Biochemistry 34*, 14230−14236.
23. Pace, C. N., Vajdos, F., Fee, L., Grimsley, G., and Gray, T. (1995) *Protein Sci. 4*, 2411−2423.
24. Popp, C. A., and Hyde, J. S. (1981) *J. Magn. Reson. 43*, 249−258.
25. Altenbach, C., Greenhalgh, D. A., Khorana, H. G., and Hubbell, W. L. (1994) *Proc. Natl. Acad. Sci. U.S.A. 91*, 1667−1671.
26. Budker, V., Du, J.-L., Seiter, M., Eaton, G. R., and Eaton, S. S. (1995) *Biophys. J. 68*, 2531−2542.
27. Rakowsky, M. H., More, K. M., Kulikov, A. V., Eaton, G. R., and Eaton, S. S. (1995) *J. Am. Chem. Soc. 117*, 2049−2057.
28. Provencher, S. W. (1976) *J. Chem. Phys. 64*, 2772−2777.

29. Lindgren, M., Eaton, G. R., Eaton, S. S., Jonsson, B.-H., Hammarstrom, P., Svensson, M., and Carlsson, U. (1997) *J. Chem. Soc., Perkin Trans. 2*, 2549−2554.
30. Rakowsky, M. H., Zecevic, A., Eaton, G. R., and Eaton, S. S. (1998) *J. Magn. Reson. 131*, 97−110.
31. Altenbach, C., Marti, T., Khorana, H. G., and Hubbell, W. L. (1990) *Science 248*, 1088−1092.
32. Farahbakhsh, Z. T., Huang, Q.-L., Ding, L.-L., Altenbach, C., Steinhoff, H.-J., Horwitz, J., and Hubbell, W. L. (1995) *Biochemistry 34*, 509−516.
33. Altenbach, C., Yang, K., Farrens, D. L., Farahbakhsh, Z. T., Khorana, H. G., and Hubbell, W. L. (1996) *Biochemistry 35*, 12470−12478.
34. Matthews, B. W. (1995) *Adv. Protein Chem. 46*, 249−278.
35. Resek, J. F., Farahbakhsh, Z. T., Hubbell, W. L., and Khorana, H. G. (1993) *Biochemistry 32*, 12025−12032.
36. Pecoraro, V. L., Wong, G. B., Kent, T. A., and Raymond, K. N. (1983) *J. Am. Chem. Soc. 105*, 4617−4623.
37. Spartalian, K., Oosterhuis, W. T., and Neilands, J. B. (1975) *J. Chem. Phys. 62*, 3538−3543.
38. Nakagawa, K., Candelaria, M. B., Chik, W. W. C., Eaton, S. S., and Eaton, G. R. (1992) *J. Magn. Reson. 98*, 81−91.
39. Seiter, M., Budker, B., Du J.-L., Eaton, G. R., and Eaton, S. S. (1998) *Inorg. Chim. Acta* (in press).
40. Karpishin, T. B., Dewey, T. M., and Raymond, K. N. (1993) *J. Am. Chem. Soc. 115*, 1842−1851.
41. Newton, S. M., Allen, J. S., Cao, Z., Qi, Z., Jiang, Z., Sprencel, C., Igo, J. D., Foster, S. B., Payne, M. A., and Klebba, P. E. (1997) *Proc. Natl. Acad. Sci. U.S.A. 94*, 4560−4565.
42. Skare, J. T., Ahmer, B. M. M., Seachord, C. L., Darveau, R. P., and Postle, K. (1993) *J. Biol. Chem. 268*, 16302−16308.
43. Larsen, R. A., Foster-Hartnett, D., McIntosh, M. A., and Postle, K. (1997) *J. Bacteriol. 179*, 3213−3221.
44. Leigh, J. S., Jr. (1970) *J. Chem. Phys. 52*, 2608−2612.
45. Voss, J., Hubbell, W. L., and Kaback, H. R. (1995a) *Proc. Natl. Acad. Sci. U.S.A. 92*, 12300−12303.
46. Voss, J., Salwinski, L., Kaback, H. R., and Hubbell, W. L. (1995b) *Proc. Natl. Acad. Sci. U.S.A. 92*, 12295−12299.
47. Eaton, S. S., and Eaton, G. R. (1988) *Coord. Chem. Rev. 83*, 29−72.
48. Hyde, J. S., Swartz, H. M., and Antholine, W. E. (1979) in *Spin Labeling II* (Berliner, L. J., Ed.) Chapter 2, pp 71−113, Academic Press, Inc., New York.
49. Bloembergen, N., Purcell, E. M., and Pound, R. V. (1948) *Phys. Rev. 73*, 679−712.

BI980144E